

1 Response to anonymous Referee #1

2

3 General Comment

4 I found that the authors have improved their manuscript based on my comment and
5 suggestion before.

6

7 Detail Comment

8 1. There are several abbreviations in the main text still do not have full name e.g. NF,
9 NW, SE, SW (Line 259-260), MILARGO (Line 263).

10 *Reply: These abbreviations that correspond to northeast, northwest, southeast and southwest,*
11 *respective, have now been included as words.*

12 *The acronym MILAGRO stands for Megacity Initiative: Local And Global Research*
13 *Observations, and has now been included in the revised text.*

14

15

16 2. Figure 1. I suggest the authors include Mexico map in insert and show which part
17 of Mexico represent the study location (sampling stations).

18 *Reply: The revised version has a map of Mexico, showing the location of Mexico City.*

19

20

21 Response to anonymous Referee #2

22

23 Using 1 000 000 hourly ozone measurements this paper makes a convincing case that
24 ozone is modulated in Mexico City by the MJO through the modulation of UV light. The
25 paper is well written and the analysis is generally sound. I have a few minor comments, but
26 after these are addressed the paper should be published.

27

28 1. Table 1 is a bit mysterious to me. I have some trouble precisely understanding the
29 procedure used from the wording "ozone concentrations at average of all 5 stations either
30 greater than the 90% percentile level or less than the 10th percentile level". At any rate the
31 numbers in the table are all around 10% which makes sense if one picks the top 10% or
32 bottom 10% of ozone. However, I don't understand what the deviations from 10% level
33 mean. Is this due to station heterogeneity? The authors should clarify the exact procedure
34 used for making this table and discuss how to interpret the findings.

35

36 *Reply: We believe the reviewer refers to Table 2 in this comment.*

37

38 The actual procedure to calculate extreme low and high ozone was described in the text in
39 section 2. Data and Methods (page 8). To define days with extreme high and extreme low
40 ozone concentrations, the following procedure as used:

41 i) The frequency distributions for the datasets of standard anomalies for the afternoon
42 (1200 to 1600 LT) for summer and for winter (using the 1986-2014 period), were
43 computed to determine the values that correspond to the 90th and 10th percentiles.

44 ii) A day with extreme low ozone concentration is determined when the average standard
45 anomaly for the 5 stations for that day is less than the 10th percentile for the season.

46 iii) A day with extreme high ozone concentration is determined when the average standard
47 anomaly for the 5 stations for that day is greater than the 90th percentile for the season.

48 iv) The extreme day identified as above is then related to the phase of the MJO, and then the
49 relative frequency is estimated from the number of extreme ozone as a fraction of the total
50 number of days in the particular phase.

51

52 We apologize for the not having a clear enough caption and we have re-written the caption
53 so it now read as follows:

54 "Table 2: Relative frequency of extreme ozone days in winter (top two rows) and summer
55 (bottom two rows). A high ozone day was defined as one with a mean afternoon (1200 to
56 1600 local) ozone anomaly across the 5 observing stations greater than the long-term
57 (1986-2014) 90th percentile. Similarly, a low ozone day was defined as one with a mean
58 afternoon anomaly across the 5 observing stations less than the long-term 10th percentile.
59 Bold values (winter phase 2; summer phase 6) indicate phases with highest mean ozone
60 concentrations in those seasons; italics in italics (winter phase 8; summer phase 1) indicate
61 phases with lowest mean ozone concentrations in those seasons. Number of days (n) in
62 each active phase is given for each season, used to estimate the relative frequency."

63

64

65 2. Line 137. I assume the 30-day basis is a moving window. Please clarify.

66

67 *Reply:* Yes, it is a running average or moving window, and we have now added this
68 information in the text in section 2. Data and Methods.
69 The basis for this choice was explained in this same section “the 30-day period was
70 selected to avoid influence from both seasonal variability and also the long-term trend.”
71

72
73 3. Line 159. ‘DFJ’ should be ‘DJF’.
74

75 *Reply:* We thank the reviewer for catching this typographical error, which has now been
76 corrected throughout the manuscript and figure captions.
77

78
79 4. Figure 5 and similar figures. It would be preferable if the projections on all panels are the
80 same.
81

82 *Reply:* Figures 5, 6, 8 and 9 have been re-done so that the panels on the first column have
83 the same projection as all other panels. They new figures have been now included in the
84 revised text.
85

86
87 5. Figure 7. How helpful is this as a forecast tool? It might be helpful to put in each figure
88 the percentage of days in each category.
89

90 *Reply:* We have not attempted to use it as a forecast tool, but it would be simple to do.
91 From the climatological work in this study, a particular phase associated with each day
92 would be associated statistically high or low ozone. That would then be compared then
93 with the normalized daily data (averaged over the 5 stations), classified as extreme high or
94 low, to determine the skill of the prediction.

95 We have chosen not to include the percentage of days in Figure 7, since it would be
96 confusing but mainly because the corresponding values were already listed in Table 2 and
97 available to readers.
98

99
100 6. Lines 379-381. It looks to me like days with high ozone feature anomalous westerly
101 winds in DJF.
102

103 *Reply:* Yes, you are right, and thank you for pointing this out. As is clearly seen in Fig 10,
104 surface westerly winds anomalies are observed during winter high O₃ events. We have
105 now corrected the text and it now reads as follows:
106

107 “In winter, days in phase 8 (lowest ozone concentrations) featured anomalous
108 northeasterly surface winds (blue vectors; Fig. 10), resulting in observed wind speeds up to
109 40% stronger than climatology (red vectors in Fig. 10). Days in phase 2 (highest ozone
110 concentrations) featured anomalous westerly winds, resulting in winds up to 50% weaker
111 in magnitude (Fig. 10) than climatology. In summer, days in phases 8 and 1 (lowest ozone
112 concentrations) featured surface winds very similar to climatology in both magnitude and

113 direction. In summer, the wind direction on days in phase 8 was more from the north-
114 northwest, while climatology was from the north-northeast, resulting in a very small
115 westerly anomaly. Days in phase 6 (highest ozone concentrations) also featured winds
116 with similar direction as the seasonal mean, but with speeds up to 30% faster (Fig. 10). “
117 |

118

119

120 **Variability of winter and summer surface ozone in Mexico City**

121 **on the intraseasonal time scale**

122

123

124

125

126 Bradford S. Barrett^{1,2} and Graciela B. Raga¹

127 ¹Centro de Ciencias de la Atmósfera, Universidad Nacional Autónoma de México, Mexico City 04510, Mexico

128 ²Oceanography Department, U.S. Naval Academy, Annapolis 21401, United States of America

129

130 *Correspondence to:* Graciela B. Raga (raga.graciela@gmail.com; raga@unam.mx)

131 **Abstract.** Surface ozone concentrations in Mexico City frequently exceed the Mexican standard
132 and have proven difficult to forecast due to changes in meteorological conditions at its tropical
133 location. The Madden-Julian Oscillation (MJO) is largely responsible for intraseasonal
134 variability in the tropics. Circulation patterns in the lower and upper troposphere and
135 precipitation are associated with the oscillation as it progresses eastward around the planet. It is
136 typically described by phases (labeled 1 through 8), which correspond to the broad longitudinal
137 location of the active component of the oscillation with enhanced precipitation. In this study we
138 evaluate the intraseasonal variability of winter and summer surface ozone concentrations in
139 Mexico City was investigated over the period 1986-2014 to determine if there is a modulation by
140 the MJO that would aid in the forecast of high pollution episodes.

141 Over 1 000 000 hourly observations of surface ozone from five stations around the metropolitan
142 area were standardized and then binned by active phase of the MJO, with phase determined using
143 the Real-time Multivariate MJO Index. Highest winter ozone concentrations were found in
144 Mexico City on days when the MJO was active and in phase 2 (over the Indian Ocean), and
145 highest summer ozone concentrations were found on days when the MJO was active and in
146 phase 6 (over the western Pacific Ocean). Lowest winter ozone concentrations were found during
147 active MJO phase 8 (over the eastern Pacific Ocean), and lowest summer ozone concentrations
148 were found during active MJO phase 1 (over the Atlantic Ocean). Anomalies of reanalysis-based
149 cloud cover and UV-B radiation supported the observed variability in surface ozone in both
150 summer and winter: MJO phases with highest ozone concentration had largest positive UV-B
151 radiation anomalies and lowest cloud cover fraction, while phases with lowest ozone
152 concentration had largest negative UV-B radiation anomalies and highest cloud cover fraction.
153 Furthermore, geopotential height anomalies at 250 hPa favoring reduced cloudiness, and thus

154 elevated surface ozone, were found in both seasons during MJO phases with above-normal ozone
155 concentrations. Similar height anomalies at 250 hPa favoring enhanced cloudiness, and thus
156 reduced surface ozone, were found in both seasons during MJO phases with below-normal ozone
157 concentrations. These anomalies confirm a physical pathway for MJO modulation of surface
158 ozone via modulation of the upper-troposphere.

159 **1 Introduction**

160 Ozone is hazardous to human health (WHO, 2008) and is a ubiquitous problem in many
161 megacities around the world. Tropospheric ozone is a secondary pollutant produced by complex
162 photochemistry from anthropogenic emissions and high ozone events typically affect mid-
163 latitude urban areas during summer, while in the tropics, such events can be observed throughout
164 the year. The problem of the incidence of high surface ozone events is exacerbated in Mexico
165 City, a megacity with 21 million inhabitants, because of the intense solar radiation received at its
166 relatively high elevation (more than 2200 m above sea level) and tropical latitude (19.4°N) (Lei
167 et al., 2007). Furthermore, the city is located in a basin, effectively preventing efficient
168 ventilation of the polluted air (Fast and Zhong, 1998; Whiteman et al., 2000; Zhang et al., 2009).

169 Seasonal variability in maximum surface ozone concentrations is not large in Mexico
170 City due to its geographical location (Raga and LeMoine, 1996). Both in the dry winter
171 (December-February) and wet summer (June-August) months, clear skies and strong insolation
172 in the morning hours promote rapid generation of surface ozone via photochemical conversions
173 from anthropogenic precursor emissions near the surface. In both seasons, as the day progresses,
174 the boundary layer becomes unstable from solar radiation and deepens, diluting pollutant
175 concentrations near the surface. The growth of the boundary layer in Mexico City occurs over
176 the course of a few hours, with typical heights reaching at least 1.2 km above the surface
177 (Nickerson et al, 1992; Perez Vidal and Raga, 1998), even during the winter months when
178 insolation is reduced at this latitude. Highest ozone concentrations during the winter months are
179 often seen on days with strong insolation and light or no surface wind (Lei et al., 2007). In
180 summer months, clouds and precipitation generally reduce the number of days with extremely
181 elevated surface ozone concentrations. However, when large-scale atmospheric conditions are

182 favorable, such as when a high pressure regime and associated clear skies affect the Mexico City
183 basin, elevated concentrations of surface ozone are also recorded in summer (Raga and Le
184 Moyne, 1996). Hourly surface ozone concentrations routinely exceed the national standard, set
185 at 110 ppb in 1993 (by law NOM-020-SSA1-1993) and modified in 2014 to 95 ppb (by law
186 NOM-020-SSA1-2014). In 2015, hourly maximum O₃ concentrations in every month of the year
187 exceeded the standard set in 2014 at monitoring stations in all five geographic regions: NE, NW,
188 SE, SW and Center (Rodríguez et al., 2016).

189 The problem of air quality in Mexico City has been the subject of numerous field
190 programs over the years, typically limited in time but more comprehensive in terms of the
191 number of parameters measured. One such campaign was MILAGRO: [Megacity Initiative: Local
192 and Global Research Observations](#), a very large international field campaign that took place in
193 March 2006. The results of the large number of publications from that project are summarized
194 by Molina et al (2010). These results provided new insight into several processes related with
195 pollutant transformations and chemical pathways, emerging from the analysis of the data
196 collected with the large suite of sophisticated instrumentation deployed and the modeling
197 performed. However, intensive field campaigns limited to one month, cannot address the
198 seasonal and intraseasonal variability of the high surface ozone within the city. Past studies
199 have examined the variability of surface ozone in Mexico City at different time scales, e.g.
200 hourly (Raga and Le Moyne, 1996; Huerta et al., 2004; Lei et al., 2007), daily (Fast and Zhong,
201 1998), weekly (Stephens et al., 2008), monthly (Rodríguez et al., 2016), and seasonal (Thompson
202 et al., 2008). All of these studies noted a primary relationship between ozone concentration in
203 Mexico City and ultraviolet (UV) radiation, where days with more UV radiation were associated
204 with elevated surface ozone concentrations. Furthermore, UV radiation received at the surface is

205 strongly modulated by cloud cover (El-Nouby Adam and Ahmed, 2016). However, as yet, no
206 study has explored surface ozone variability in Mexico City on the intraseasonal (30-60 day)
207 time scale, despite known relationships between the leading mode of atmospheric intraseasonal
208 variability, the Madden-Julian Oscillation (MJO; Madden and Julian, 1971), and tropical cloud
209 cover (Riley et al., 2011) and circulation (Madden and Julian, 1972; Zhang, 2005). The MJO is
210 largely responsible for intraseasonal variability in the tropics. Circulation patterns in the lower
211 and upper troposphere and precipitation are associated with the oscillation as it progresses
212 eastward around the planet. It is typically described by phases (labeled 1 through 8), which
213 correspond to the broad longitudinal location of the active component of the oscillation with
214 enhanced precipitation.

215 In this study we evaluate the intraseasonal variability of winter and summer surface
216 ozone concentrations in Mexico City over the period 1986-2014 to determine if there is a
217 modulation by the MJO that would aid in the forecast of high pollution episodes. Based on the
218 relationships between surface ozone and UV radiation, UV radiation and cloud cover, and cloud
219 cover and the MJO, the primary hypothesis tested in this study was the following: *surface ozone*
220 *varies intraseasonally by phase of the MJO.*

221 The physical pathway hypothesized to support this intraseasonal variability was as
222 follows: *anomalies in tropical convection associated with the MJO drive variability in upper*
223 *tropospheric circulation, and that variability can be seen in composite anomalies of height and*
224 *wind by MJO phase* (e.g., Madden and Julian, 1994; Zhang, 2005). Those circulation anomalies
225 then drive variability in cloud cover and thus variability in UV radiation reaching the boundary
226 layer, which in turn is seen in phase-to-phase variability in surface ozone concentrations in
227 Mexico City. The cloud-UV radiation portion of our hypothesis is supported by Kerr et al.

228 (2008), who found that typical UV transmission ratios range between 0.3 and 0.8 for overcast
229 conditions (Cede et al., 2002) and as little as 0.05 for thick cumulonimbus clouds (McArthur et
230 al., 1999). It is also supported by An et al. (2008), who found a strong relationship between
231 surface ozone concentrations in Beijing and surface UV radiation, particularly in summer, and
232 noted that surface UV was up to 200% more sensitive to total cloud cover than was surface total
233 radiation. The motivation to explore potential relationships between the MJO and surface ozone
234 concentrations came from Barrett et al. (2012), who found differences as large as 25% of the
235 daily mean in afternoon summer ozone concentrations in Santiago, Chile, by phase of the MJO
236 and tied those differences to changes in cloud fraction associated with synoptic-scale circulation
237 variability in different MJO phases.

238

239 **2 Data and methods**

240 The government monitoring network, Red Automática de Monitoreo Atmosférico
241 (Automated Atmospheric Monitoring Network, RAMA) has been operational since January 1986
242 measuring all criteria pollutants, with instrumentation certified by the US Environmental
243 Protection Agency (EPA). In particular, the instrument to measure ozone is produced by Thermo
244 Environmental Instrument Model 49, by UV absorbance. The RAMA currently has 33 stations
245 within the Mexico City basin, but only a few have records dating back to 1986.

246 We selected five stations with the longest periods of record (Table 1), one station from
247 each of the five geographic regions in the metropolitan area identified by several previous studies
248 and summarized by Raga et al. (2001). Hourly observations from Tlalnepantla (TLA, in the
249 [northwest sector of the city](#), NW), Xalostoc (XAL, in the [northeast sector](#), NE), Merced (MER,
250 in the Center), Pedregal (PED, in the [southwest sector](#), SW), and Universidad Autónoma

251 | Metropolitana-Iztapalapa (UIZ, in the [southeast sector](#), SE) were available beginning in January
252 | 1986 and up to December 2014. See Figure 1 for station locations and Table 1 for numbers of
253 | observations and elevations of each station. Since the ozone time series were non-stationary,
254 | standard anomalies (also called normalized anomalies) were calculated by subtracting a mean
255 | value from each observation and then dividing that result by a standard deviation (Wilks, 2011).
256 | Those mean values and standard deviations for each hour were [estimated applying a 30-day](#)
257 | (approximately monthly) [running window](#), and the 30-day period was selected to avoid influence
258 | from both seasonal variability and also the long-term trend. We did not stratify by day of the
259 | week based on Stephens et al. (2008), who found that ozone in Mexico City exhibited relatively
260 | little variability by day of the week. Furthermore, we defined a “low” ozone concentration day
261 | as one with mean afternoon (1200 to 1600 local time) ozone standard anomalies (averaged across
262 | the five observing stations) below the 10th percentile. Percentiles were determined separately for
263 | each season using standard anomalies on all days in that season from 1986 to 2014. Similarly, we
264 | defined a “high” ozone concentration day as one where mean afternoon ozone standard
265 | anomalies exceeded the 90th percentile, again calculating winter and summer percentiles
266 | separately.

267 | The MJO phase was determined using the Real-time Multivariate MJO (RMM) index
268 | (Wheeler and Hendon, 2004). The daily RMM is based on time series of two principal
269 | components derived from empirical orthogonal functions of equatorially (5°S to 5°N) averaged
270 | 200-hPa zonal wind, 850-hPa zonal wind, and outgoing longwave radiation. The projection of
271 | daily data onto the empirical orthogonal functions serves as a time filter and makes the RMM
272 | useful in a real-time setting (Wheeler and Hendon, 2004). The RMM is divided into eight phases,
273 | and each phase corresponds to the broad geographic location of the MJO tropical convective

graciela binimelis d..., 14/10/16 8:41 A.M.
Eliminado: calculated on
graciela binimelis d..., 14/10/16 8:41 A.M.
Eliminado: basis

276 signal on that day. An active MJO was defined in this study as one with RMM amplitude, which
277 is the square root of the sum of the squares of the two principal components RMM1 and RMM2
278 (Wheeler and Hendon, 2004), greater than 1.0 (LaFleur et al., 2015). Each day's hourly standard
279 ozone anomalies were binned using the phase of active MJO of that day. Mean values for each
280 MJO phase were then calculated, first annually and then for each season (DJF, and JJA).

281 Values of geopotential height (in m) and u - and v vector wind components at 250 hPa (in
282 m s^{-1}), along with total cloud cover, high cloud cover, and low cloud cover (expressed as
283 fractions from 0 to 1) and downward UV radiation received at the surface (UV-B, in W m^{-2}) at
284 1800 UTC (1200 local time) were derived from the ERA-Interim reanalysis (Dee et al., 2011).
285 We chose to examine 250 hPa in part based on the results of Li et al. (2012), who connected
286 intraseasonal ozone variability across east Asia with variability in upper-troposphere
287 geopotential heights by MJO phase. Additionally, we are aware that cloud cover in reanalysis has
288 biases, and we selected the ERA-Interim product because it specifically includes an improved
289 deep convective cloud triggering mechanism over tropical land masses (Bechtold et al., 2004)
290 and thus shows skill over other products (Dee et al., 2011).

291 We selected the winter (Dec-Feb; DJF) and summer (June-August; JJA) seasons for this
292 study because of the homogeneity in synoptic-scale weather patterns in those seasons. More
293 details on the climatological variability of ozone in Mexico City can be found in Klaus et al.
294 (2001).

295 Finally, daily values of surface wind at the Tacubaya station (TCBY in Fig. 1) were taken
296 from the NOAA National Centers for Environmental Information (NCEI) Integrated Surface
297 Database (ISD; Smith et al., 2011). Anomalies of those values, calculated with respect to
298 seasonal means, were binned by MJO phase to give composite anomalies for each season. For

graciela binimelis d..., 12/10/16 2:01 P.M.

Eliminado: J

300 UV and total cloud cover in Mexico City itself, the gridded ERA-Interim value at the point
301 closest to the mean latitude and longitude of the five RAMA stations was selected.

302

303 **3 Results**

304 **3.1 Variability of the ozone time series**

305 The diurnal cycle of ozone concentrations at each of the stations exhibited a daily
306 minimum around 0700 local time just prior to sunrise and a peak between 1200 and 1500 local
307 time, with highest concentrations at the southern-most stations (PED and UIZ) and lowest in the
308 northern-most station (XAL) (Fig. 2a). Additionally, highest ozone concentrations occurred one
309 to two hours earlier in spring (March-May; MAM) than in winter (December-February; DJF) at
310 both PED and XAL (Fig. 2b), and peak ozone at PED in the south occurred one to two hours
311 after peak ozone in XAL in the north, as a result of weak northeasterly surface winds
312 transporting ozone and photochemical precursors southward during the day (Bossert 1997).

313 Mean ozone concentrations in spring were nearly 30% higher at all stations than the rest
314 of the year (Fig. 3, with observations smoothed by a 30-day running mean), and the effects of
315 increased UV radiation during the “mid-summer drought” (*canícula*) (Magaña et al. 1999) were
316 reflected as a secondary peak in ozone concentrations in August. Minimum O₃ concentrations
317 were observed in all five stations during September, when daily maximum precipitation was
318 observed in Mexico City.

319 One of the challenges in examining intraseasonal variability of ozone is the need for a
320 stationary record over a long period. In Mexico City, ozone concentrations have steadily
321 decreased from the early 1990s to the 2010s (Fig. 4a; also Rodríguez et al., 2016) as a result of
322 pollution control measures (Molina and Molina, 2004). In order to remove the long-term trend,

323 while keeping the intraseasonal variability at hourly resolution, hourly observations were
324 converted to standard anomalies as described in Section 2. Results of this transformation of
325 hourly observations to standard anomalies for station PED are shown in Figures 4a (original
326 hourly observations) and 4c (hourly standard anomalies). Standard anomalies for the other four
327 stations show very similar results.

328 We note that overnight minimum observations from 1991 to 1993 were probably
329 overestimated in the observational record (Fig. 4a), an artifact also seen in the other four stations
330 (not shown). However, because in this study we focused on afternoon values (from 1200 to 1600
331 local time), that potential overestimation did not materially impact our results.

332 By transforming each hourly observation into a standard anomaly, the distribution of
333 relative frequencies shifted from highly non-Gaussian, with peaks near zero and very long right
334 tails (Fig. 4b), to more Gaussian, with peaks near -0.5 and reduced skewness (Fig. 4d). Although
335 the peaks in these transformed distributions were less than zero, and the right tails were longer
336 than the left tails, the means of each of the distributions of standard anomalies in Figure 4d were
337 very near zero, falling between -0.03 and 0.

338

339 **3.2 Synoptic patterns associated with low and high ozone**

340 Before examining ozone variability by MJO phase, it was important to first establish the
341 synoptic-scale patterns associated with days of low and high ozone concentrations (defined in
342 Section 2) in each season.

343 In winter (DJF), the synoptic pattern on days with low afternoon surface ozone
344 concentration featured a 250-hPa ridge over northwest Mexico and the southwest U.S. (height
345 anomalies up to +50 m) and a 250-hPa trough over central, eastern, and southern Mexico and the

346 southern and eastern U.S. (height anomalies -10 to -40 m) (Fig. 5a). Mean circulation at 250-hPa
347 on low DJF ozone days was nearly westerly off the central Mexican west coast turning to
348 southwesterly over central Mexico (Fig. 5a). This synoptic pattern would favor enhanced
349 cloudiness over Mexico City (and thus reduced UV radiation and lower ozone concentrations)
350 via two mechanisms: first, through quasi-geostrophic ascent associated with the 250-hPa trough,
351 and second, through advection of moisture and high-level clouds from the subtropical Pacific
352 (around 20°N) associated with westerly and west-northwesterly winds (Fig. 5a). Indeed, positive
353 total cloud fraction anomalies were seen with this height and circulation pattern, and those cloud
354 fraction anomalies (+0.05 to +0.10) extended over central and southern Mexico and
355 northeastward into the Gulf of Mexico (Fig. 5b). Those anomalies were likely comprised
356 primarily of high cloud (+0.05 to +0.15; Fig. 5c), given the resemblance between the pattern of
357 total cloud cover (Fig. 5b) and high cloud cover (Fig. 5c). A region of positive low cloud cover
358 anomalies (up to +0.15; Fig. 5d) was also seen in central Mexico on winter days with lowest O₃
359 concentrations, likely associated with surface wind convergence over the Sierra Madre Oriental
360 Mountains, although low cloud fraction anomalies over Mexico City itself were less than +0.05.

361 The synoptic pattern for winter days with high surface ozone concentration was opposite
362 that for the low ozone days. Over northwest Mexico and the southwest U.S., a trough was seen at
363 250-hPa (anomalies -10 to -70 m), while a ridge was seen over central, southern, and eastern
364 Mexico and the southern and eastern U.S. (anomalies to +50 m; Fig. 5e). Circulation at 250 hPa
365 over central Mexico was southwesterly (compared to westerly for low ozone days). Negative
366 total cloud fraction anomalies (-0.05 to -0.15) over central and southern Mexico were associated
367 with this circulation pattern (Fig. 5f). This pattern would promote clearer than normal skies (and
368 thus enhanced UV radiation and surface ozone production) by both favoring quasi-geostrophic

369 subsidence over central Mexico (associated with the above-normal heights and ridging at 250
370 hPa) and by advecting dry, cloud-free air toward central Mexico from the tropical East Pacific
371 Ocean originating near 10°N (Fig. 5g). Similar to low ozone days, most of the negative total
372 cloud fraction anomalies were likely result of the reduction in the presence of high cloud (Fig.
373 5g), given similarity of the anomaly patterns between total (Fig. 5f) and high (Fig. 5g) cloud
374 fraction. The low cloud fraction anomaly over Mexico City itself (Fig. 5h) was close to zero,
375 although negative low cloud fraction anomalies (-0.05 to -0.15) were seen over the low-land
376 states bordering the Gulf of Mexico (Fig. 5h).

377 Summer days with low surface ozone concentration featured a slight anomalous ridge
378 (height anomalies of +5 to +15 m) over northern Mexico and much of the U.S. (Fig. 6a). This
379 synoptic-scale pattern would favor cloudiness because positive geopotential height anomalies at
380 250 hPa over northern Mexico and the southwest U.S. would be associated with a stronger
381 summer anticyclone, signifying a more intense monsoon circulation, easterly winds at 250 hPa in
382 central and southern Mexico (Fig. 6a), and precipitation in central and southern Mexico. Indeed,
383 low ozone days featured positive anomalies in total cloud fraction (Fig. 6b), high cloud fraction
384 (Fig. 6c), and low cloud fraction (Fig. 6d), with anomalies of each fractional cloud cover variable
385 ranging from +0.05 to +0.15. The regions of positive total and high cloud cover anomalies
386 extended over much of central Mexico, but anomalies in low cloud fraction were confined to
387 Mexico City and the states bordering it (Fig. 6d). Summer days with high ozone concentration
388 featured less ridging over northwestern Mexico and the southwest U.S., with 250-hPa height
389 anomalies of -10 to -20 m (Fig. 6e). This synoptic-scale pattern with weaker ridging over
390 northwest Mexico and the southwest U.S., and stronger ridging over Central America, is
391 opposite of the climatological monsoon circulation and would favor less precipitation in central

392 Mexico. Indeed, negative anomalies in fraction of total cloud cover (Fig. 6f), high cloud cover
393 (Fig. 6g), and low cloud cover (Fig. 6h) were seen on days with high ozone concentrations, with
394 anomaly magnitudes of -0.05 to -0.15 over much of central and southern Mexico (total and high
395 cloud cover) and the states bordering Mexico City and along the Sierra Madre Occidental
396 mountains (Fig. 6h). In the next section, these seasonal ozone pattern composites are compared
397 to pattern composites for MJO phases with greatest ozone anomalies.

398

399 **3.3 Intraseasonal ozone variability**

400 On an annual basis, afternoon (1200 to 1600 local time) surface ozone concentrations in
401 Mexico City were found to vary by MJO phase. Highest ozone concentrations were noted on
402 days when MJO was active and in phases 3, 4, and 5, while lowest ozone concentrations were
403 noted on days when the MJO was active and in phases 1 and 2 (Fig. 7a). This variability was
404 seen at all five stations, regardless of geographic position within the basin. Normalized
405 anomalies of surface UV radiation and total cloud fraction from ERA-Interim reanalysis strongly
406 supported the observed surface ozone variability: MJO phases with highest ozone concentrations
407 also had highest UV anomalies and lowest total cloud fraction anomalies, while MJO phases
408 with lowest ozone concentrations had the most negative UV and the most positive cloud fraction
409 anomalies (Fig. 7d). We found this agreement remarkable, particularly so because the two data
410 sets independently presented the same intraseasonal pattern.

411 On a seasonal basis, surface ozone concentrations in Mexico City were also found to vary
412 by MJO phase. However, the dependence on phase was found to change between winter and
413 summer, meaning a phase associated with higher ozone concentrations in winter would not
414 necessarily be associated with higher ozone concentrations in summer. We attribute these

415 differences to seasonality in both the convective properties of the MJO itself (e.g., Zhang and
416 Dong, 2004; Wu et al., 2006) and in the extratropical atmosphere, whose circulation the MJO
417 modulates (Gloeckler and Roundy, 2013). Despite the phase-to-phase variability in maximum
418 and minimum ozone concentrations throughout the year, in all seasons, there remained good
419 agreement between phases with highest (lowest) ozone concentrations and phases with highest
420 (lowest) UV and lowest (highest) total cloud fraction. That is, the sunnier phases were
421 consistently associated with the highest ozone concentrations.

422 In winter months (DJF), highest ozone concentrations were found on days when the MJO
423 was in phase 2, and lowest ozone concentrations were found on days when the MJO was in phase
424 8 (Fig. 7b). Highest UV radiation, and lowest total cloud fraction, were seen on days when the
425 MJO was in phase 2, and lowest UV radiation and second-highest cloud fraction were seen on
426 days when the MJO was in phase 8 (Fig. 7e). In summer months (JJA), highest ozone
427 concentrations were found on days when the MJO was in phases 5, 6, and 7, and lowest ozone
428 concentrations were found on days when the MJO was in phases 1 and 8 (Fig. 7c). Highest UV
429 radiation, and lowest total cloud fraction, was seen on days when the MJO was in phase 6, and
430 lowest UV radiation and highest total cloud fraction were seen on days when the MJO was in
431 phase 1. In both winter and summer, UV radiation and cloud cover anomalies strongly supported
432 observed surface ozone anomalies, whereby the cloudiest MJO phases featured lowest ozone and
433 the sunniest phases featured highest ozone. We again consider this agreement remarkable, given
434 the independence of the ozone and reanalysis data sets. Summer months (JJA) featured the
435 greatest range in mean ozone concentrations by MJO phase: a difference in 0.25 standard
436 anomaly units between the phases with the highest ozone concentrations (phases 5 and 6) and the

437 phases with the lowest ozone concentrations (phases 1 and 8) (Fig. 7c). Summer months also
438 featured the largest spread in both UV and total cloud fraction standard anomalies (Fig. 7f).

439 An examination of the frequency of “extreme” ozone days in each MJO phase (here a day
440 with an “extreme” ozone value was defined for each season as an afternoon standard anomaly
441 either above the 90th percentile value or below the 10th percentile value) provides additional
442 insight into the character of the MJO modulation of ozone. In both winter and summer, the
443 phases associated with highest ozone concentrations (phase 2 in winter and phase 6 in summer)
444 featured the fewest occurrences of days with extremely low ozone (days with concentrations
445 below the 10th percentile; Table 2). Those phases also featured either the highest (in summer) or
446 near-highest (in winter) occurrences of days with concentrations above the 90th percentile (Table
447 2). Furthermore, the phases associated with lowest ozone concentration (phase 8 in winter and
448 phase 1 in summer) featured the highest occurrences of days with low ozone (Table 2) and
449 below-normal occurrence of days with high ozone. These results confirm that one manner in
450 which the MJO modulates ozone concentration in Mexico City is to reduce (or augment) the
451 frequency of days with afternoon ozone concentrations either below the 10th or above the 90th
452 percentiles.

453 To examine physical mechanisms for the observed variability in ozone concentration and
454 cloud cover by MJO phase, composite anomalies of 250-hPa height and *u*- and *v*- wind
455 components were created for each active MJO phase for each season. Seasonal anomalies of total
456 cloud fraction, high cloud fraction, and low cloud fraction were also composited for each active
457 MJO phase. In both seasons, anomalies of each variable were found for all eight MJO phases.
458 However, for the remainder of this paper, we focus only on the synoptic-scale conditions in
459 phases with maximum and minimum surface ozone. In DJF, minimum ozone concentrations

460 occurred on days when the MJO was active and in phase 8. In that phase, anomalous 250-hPa
461 ridging was seen over northwest Mexico and the southwest U.S. (anomalies up to +50 m) and
462 anomalous 250-hPa troughing over northeast Mexico and the southeastern U.S. (anomalies to -60
463 m) (Fig. 8a). This height pattern resembled the seasonal pattern for winter days with above-
464 normal cloudiness and low ozone (Figs. 5a), with troughing over central Mexico favoring both
465 cloud formation via ascent and cloud advection from the subtropical East Pacific Ocean. Indeed,
466 on days in MJO phase 8, total cloud cover anomalies were positive over nearly all of Mexico,
467 ranging from +0.05 to +0.15 (Fig. 8b). Anomalies in high cloud cover were smaller in magnitude
468 (up to +0.05), and over Mexico City, high cloud cover anomalies were zero (Fig. 8c). Positive
469 low cloud anomalies were confined to the states to the east of Mexico City (Fig. 8d), which when
470 combined with high cloud cover anomalies, suggest that the anomalies in total cloud cover (Fig.
471 8b) were composed of anomalies at multiple levels.

472 Maximum winter ozone concentrations occurred on days when the MJO was active and
473 in phase 2, and on those days, a synoptic-scale pattern opposite to that of phase 8 was seen:
474 anomalous 250-hPa troughing was seen over northern Mexico and the south-central U.S. (height
475 anomalies of -10 to -30 m) and anomalous 250-hPa ridging was seen over central and southern
476 Mexico and Central America (height anomalies +5 to +20 m) (Fig. 8e). This height pattern
477 resembled the seasonal pattern for high ozone and low cloud fraction (Fig. 5e), with anomalous
478 ridging favoring clearer than normal skies via subsidence and advection of dry air from the
479 tropical East Pacific. Indeed, below-normal total cloud fraction (anomalies -0.05 to -0.15; Fig.
480 8f), high cloud fraction (anomalies -0.05 to -0.15; Fig. 8g), and low cloud fraction (anomalies -
481 0.05 to -0.10; Fig. 8h) were seen on days when the MJO was in phase 2 over much of central and
482 southern Mexico.

483 In JJA, minimum ozone concentrations occurred on days when the MJO was in phase 1.
484 In that phase, anomalous 250-hPa ridging was seen over northwest Mexico and the southwest
485 U.S. (anomalies up to +20 m) and anomalous 250-hPa troughing in the tropical East Pacific
486 Ocean (anomalies to -20 m) (Fig. 9a). This height pattern resembled the seasonal pattern for
487 summer days associated with below-normal cloudiness and high ozone (Figs. 6a), with ridging to
488 the north characteristic of the summer monsoon in central Mexico. Indeed, above-normal total
489 cloud fraction (+0.05 to +0.15; Fig. 9b), above-normal high cloud fraction (+0.05 to +0.15; Fig.
490 9c), and above-normal low cloud fraction (+0.05 to +0.10; Fig. 9d) were seen over central and
491 southern Mexico for days in MJO phase 1. Summer maximum ozone concentrations were seen
492 on days when the MJO was in phase 6. In that phase, a weaker-than-normal ridge at 250 hPa was
493 seen as anomalous heights of -10 to -20 m over much of central Mexico (Fig. 9e). This height
494 pattern resembled the seasonal pattern for summer days associated with above-normal cloudiness
495 and high ozone (Figs. 6e), as it is largely opposite of that which characterizes the central Mexico
496 summer monsoon. Indeed, below-normal total cloud fraction (-0.05 to -0.15; Fig. 9f), high cloud
497 fraction (-0.05 to -0.15; Fig. 9g), and low cloud fraction (-0.05; Fig. 9h) were all seen on days
498 when the MJO was in phase 6.

499 The final physical variable examined for intraseasonal variability by MJO phase was the
500 surface wind vector at 1800 UTC (1200 local time) at Tacubaya (TCBY in Fig. 1) in the center-
501 west portion of the metropolitan area (Fig. 1). In winter, days in phase 8 (lowest ozone
502 concentrations) featured anomalous northeasterly surface winds (blue vectors; Fig. 10), resulting
503 in observed wind speeds up to 40% stronger than climatology (red vectors in Fig. 10). Days in
504 phase 2 (highest ozone concentrations) featured anomalous westerly winds, resulting in winds up
505 to 50% weaker in magnitude (Fig. 10) than climatology. In summer, days in phases 8 and 1

506 (lowest ozone concentrations) featured surface winds very similar to climatology in both
507 magnitude and direction. In summer, the wind direction on days in phase 8 was more from the
508 north-northwest, while climatology was from the north-northeast, resulting in a very small
509 westerly anomaly. Days in phase 6 (highest ozone concentrations) also featured winds with
510 similar direction as the seasonal mean, but with speeds up to 30% faster (Fig. 10). Despite these
511 variations by MJO phase across all seasons, we do not consider the surface wind anomalies to be
512 physically consistent or representative of a large-scale pattern, for two reasons. First, because
513 Mexico City is located in a basin, surface flow fields do not normally respond to synoptic-scale
514 pattern variability (Stephens et al., 2008). Indeed, the majority of the day-to-day variability in
515 surface wind speed and direction is controlled by mesoscale, thermally-driven mountain-valley
516 circulations (Doran et al., 1998). With the exception of “cold surge” events in winter that have
517 been associated with cloudy days, the two dominant ozone patterns identified by De Foy et al.
518 (2005) only served to identify whether the ozone maximum would be in the southern or northern
519 parts of the metropolitan area. Second, the wind anomalies by MJO phase resulted in only subtle
520 changes in either direction, or speed, or both (Fig. 10). Moreover, none of the wind anomalies
521 identified in DJF would meet the northerly “cold surge” of De Foy et al. (2005), suggesting that
522 the “cold surge” events can occur during different MJO phases unrelated to modulation from the
523 MJO. Finally, the smallness of the surface wind variability by MJO phase supports our argument
524 that variability in surface ozone concentrations by MJO phase are primarily driven by variability
525 in total cloud cover and surface UV radiation, which in turn are related to anomalies in upper-
526 tropospheric circulation.

527

528 4 Conclusions

graciela binimelis d..., 14/10/16 8:51 A.M.

Eliminado: In winter, days in phase 8 (lowest ozone concentrations) featured anomalous westerly surface winds (blue vectors; Fig. 10), resulting in observed wind speeds up to 50% weaker than climatology (red vectors in Fig. 10). Days in phase 2 (highest ozone concentrations) featured small or weakly anomalous easterly winds, resulting in winds similar to climatology but up to 40% stronger in magnitude (Fig. 10). In summer, days in phases 8 and 1 (lowest ozone concentrations) featured surface winds very similar to climatology in both magnitude and direction. In summer, the wind direction on days in phase 8 was more from the north-northwest, while climatology was from the north-northeast. Days in phase 6 (highest ozone concentrations) also featured winds with similar direction as the seasonal mean, but with speeds up to 30% faster (Fig. 10).

graciela binimelis d..., 14/10/16 8:51 A.M.

Eliminado:

547 In this study, we investigated the intraseasonal variability of winter (DJF) and summer
548 (JJA) surface ozone concentrations in Mexico City. After standardizing over 1 000 000 hourly
549 observations of surface ozone from five stations around the metropolitan area, we binned them
550 by phase of the active MJO. We found that highest winter ozone concentrations occurred on days
551 when the MJO was active and in phase 2 (in the Indian Ocean), and highest summer ozone
552 concentrations occurred on days when the MJO was active and in phase 6 (in the western Pacific
553 Ocean) in summer. Lowest ozone concentrations were found on winter days in MJO phase 8 (in
554 the eastern Pacific Ocean) and summer phase 1 (in the Atlantic Ocean). This intraseasonal
555 variability in surface ozone concentrations agreed well with anomalies in cloud cover and UV-B
556 radiation: phases with highest ozone concentration had highest UV-B radiation and lowest cloud
557 cover, while phases with lowest ozone concentration had lowest UV-B radiation and highest
558 cloud cover. This agreement was found for both winter and summer. Circulation anomalies at
559 250 hPa were found to support the observed variability in ozone and cloud cover. In winter,
560 height and circulation anomalies favoring reduced cloudiness, and thus elevated surface ozone,
561 were found on days when the MJO was in phase 2, and height and circulation anomalies favoring
562 enhanced cloudiness, and thus reduced surface ozone, were found on days when the MJO was in
563 phase 8. In summer, monsoon-like 250-hPa circulation patterns that favor enhanced cloudiness,
564 and thus reduced surface ozone, were found on days when the MJO was in phase 1, and 250-hPa
565 circulation patterns opposite to the monsoon, favoring reduced cloudiness and thus elevated
566 surface ozone, were found on days when the MJO was in phase 6. We did not find physically
567 meaningful variability in surface wind direction by MJO phase, despite earlier studies suggesting
568 a relationship between surface wind and surface ozone in Mexico City. This suggests that the

569 intraseasonal variability in both summer and winter surface ozone by MJO phase is driven
570 primarily by variability in cloud cover via modulation of upper-troposphere circulation.

571

572

573 *Acknowledgements*

574 Partial funding for B. Barrett was provided by the Fulbright Scholar program of the U.S.
575 State Department and the Programa de Estancias de Investigación, Dirección General de
576 Personal Académico, Universidad Nacional Autónoma de México (DGAPA-UNAM). The air
577 quality data were obtained from the databases of the Mexico City's Air Quality Monitoring
578 Network operated by the Ministry of Environment of Mexico City. ERA-Interim data were
579 provided courtesy of ECMWF.

580 **References**

- 581 An, J. L., Wang, Y. S., Li, X., Sun, Y., and Shen, S H.: Relationship between surface UV
582 radiation and air pollution in Beijing (in Chinese). *Environ. Sci*, 29, 1054-1058, 2008.
- 583 Barrett, B. S., Fitzmaurice, S. J., and Pritchard S. R.: Intraseasonal variability of surface ozone in
584 Santiago, Chile: modulation by phase of the Madden-Julian Oscillation (MJO). *Atmos.*
585 *Environ.*, 55, 55-62, 2012.
- 586 Bechtold, P., Chaboureaud, J. P., Beljaars, A. C. M., Betts, A. K., Kohler, M., Miller, M.,
587 Redelsperger, J.-L.: The simulation of the diurnal cycle of convective precipitation over
588 land in a global model. *Q. J. R. Meteorol. Soc.*, 130, 3119–3137, 2004.
- 589 Bossert, J. E.: An investigation of flow regimes affecting the Mexico City Region. *J. Applied*
590 *Meteor.*, 36(2), 119-140, 1997.
- 591 Cede, A., Blumthaler, M., Luccini, E., Piacentini, R. D., and Numez, L.: Effects of clouds on
592 erythemal and total irradiance as derived from data of the Argentine Network. *Geophys.*
593 *Res. Lett*, 29, doi:10.1029/2002GL015708, 2002.
- 594 Dee, D. P., and Co-authors: The ERA-Interim reanalysis: configuration and performance of the
595 data assimilation system. *Q. J. R. Meteorol. Soc.*, 137, 553-597, 2011.
- 596 De Foy, B., Caetano, E., Magaña, V., Zitácuaro, A., Cárdenas, B., Retama, A., Ramos, R.,
597 Molina, L. T., and Molina, M. J.: Mexico City basin wind circulation during the MCMA-
598 2003 field campaign. *Atmos. Chem. Phys.*, 5, 2267-2288, 2005.
- 599 Doran, J. C., Abbot, S., Archuleta, J., and Bian, X.: The IMADA-AVER boundary layer
600 experiment in the Mexico City area. *Bull. Amer. Meteor. Soc.*, 79, 2497-2508, 1998.

601 El-Nouby Adam, M. and Ahmed, E. A.: An assessment of the ratio of ultraviolet-B to broadband
602 solar radiation under all cloud conditions at a subtropical location. *Adv. Space Res.*,
603 57(3), 764-775, 2016.

604 Fast, J. D. and Zhong, S.: Meteorological factors associated with inhomogeneous ozone
605 concentrations within the Mexico City basin. *J. Geophys. Res.*, 103(D15), 18927-18946,
606 1998.

607 Gloeckler, L. C. and Roundy, P. E.: Modulation of the extratropical circulation by combined
608 activity of the Madden-Julian Oscillation and equatorial Rossby waves during boreal
609 winter. *Mon. Wea. Rev.*, 141, 1347-1357, 2013.

610 Huerta, G., Sansó, B., and Stroud, J. R.: A spatiotemporal model for Mexico City ozone levels.
611 *Appl. Statist.*, 53(2), 231-248, 2004.

612 Kerr, J. B., and Fioletov, V. E.: Surface ultraviolet radiation. *Atmos.-Ocean*, 46, 159-184, 2008.

613 Klaus, D., Poth, A., Voss, M. and Jáuregui, E.: Ozone distributions in Mexico City using
614 principal component analysis and its relation to meteorological parameters. *Atmósfera*,
615 14(4), 171-188, 2001.

616 LaFleur, D. M., Barrett, B. S., and Henderson, G. R.: Some climatological aspects of the
617 Madden-Julian Oscillation (MJO). *J. Climate*, 28, 6039-6053, 2015.

618 Lei, W., de Foy, B., Zavala, M., Volkamer, R., and Molina, L. T.: Characterizing ozone
619 production in the Mexico City Metropolitan Area: a case study using a chemical transport
620 model. *Atmos. Chem. Phys.*, 7, 1347-1366, 2007.

621 Li, K.-F., Tian, B., Waliser, D. E., Schwartz, M. J., Neu, J. L., Worden, J. R., and Yung, Y. L.:
622 Vertical structure of MJO-related subtropical ozone variations from MLS, TES, and
623 SHADOZ data. *Atmos. Chem. Phys.*, 12, 425-436, 2012.

624 Madden, R. and Julian, P.: Detection of a 40-50 day oscillation in the zonal wind in the tropical
625 Pacific, *J. Atmos. Sci.*, 28, 702-708, 1971.

626 Madden, R. and Julian, P.: Description of global-scale circulation cells in the tropics with a 40-
627 50 day period. *J. Atmos. Sci.*, 29, 1109-1123, 1972.

628 Madden, R. and Julian, P.: Observations of the 40-50 day tropical oscillation: a review. *Mon.*
629 *Wea. Rev.*, 122, 814-837, 1994.

630 Magaña, V., Amador, J. A., and Medina, S.: The midsummer drought over Mexico and Central
631 America. *J. Climate*, 12(6), 1577-1588, 1999.

632 McArthur, L. J. B., Fioletov, V. E., Kerr, J. B., McElroy, C. T., and Wardle, D. I. Derivation of
633 UV-A irradiance from pyranometer measurements. *J. Geophys. Res.*, 104, 1999.

634 Molina, L. T., S. Madronich, J. S. Gaffney, E. Apel, B. de Foy, J. Fast, R. Ferrare, S. Herndon, J.
635 L. Jimenez, B. Lamb, A. R. Osornio-Vargas, P. Russell, J. J. Schauer, P. S. Stevens, R.
636 Volkamer, and M. Zavala: An overview of the MILAGRO 2006 Campaign: Mexico City
637 emissions and their transport and transformation. *Atmos. Chem. Phys.*, 10, 8697-8760,
638 2010.

639 Molina, L. T. and Molina, M. J.: Improving air quality in megacities: Mexico City case study.
640 *Annals of the New York Acad. Sci.*, 1023, 142-158, 2004.

641 Nickerson, C. E., Sosa, G., Hochstein, H., MacCaslin, P., Luke, W., and Schanot, A.:
642 Measurements of Mexico City air pollution by a research aircraft. *Atmos. Environ.*, 26B,
643 445-451, 1992.

644 Perez Vidal, H. and Raga, G. B.: On the vertical distribution of pollutants in Mexico City.
645 *Atmósfera*, 11, 95-108, 1998.

646 Raga, G. B. and Le Moyne, L.: On the nature of air pollution dynamics in Mexico City—I.
647 Nonlinear analysis. *Atmos. Environ.*, 30(23), 3987-3993, 1996.

648 Raga, G. B., Baumgardner, D., Castro, T., Martinez-Arroyo, A., and Navarro-Gonzalez, R.:
649 Mexico City air quality: A qualitative review of gas and aerosol measurements (1960-
650 2000). *Atmos. Environ.*, 35, 4041-4058, 2001.

651 Riley, E. M., Mapes, B. E., and Tulich, S. N.: Clouds associated with the Madden-Julian
652 Oscillation: a new perspective from CloudSat. *J. Atmos. Sci.*, 68, 3032-3061, 2011.

653 Rodríguez, S., Huerta, G., and Reyes, H.: A study of trends for Mexico City ozone extremes:
654 2001-2014. *Atmósfera*, 29(2), 107-120, 2016.

655 Smith, A., Lott, N., and Vose, R.: The Integrated Surface Database: Recent Developments and
656 Partnerships. *Bull. Amer. Meteor. Soc.*, 92, 704–708, 2011.

657 Stephens, S., Madronich, S., Wu, F., Olson, J. B., Ramos, R., Retama, A., and Muñoz, R.:
658 Weekly patterns of México City’s surface ozone concentrations of CO, NO_x, PM₁₀ and
659 O₃ during 1986-2007. *Atmos. Chem. Phys.*, 8, 5313-5325, 2008.

660 Thompson, A. M., Yorks, J. E., Miller, S. K., Witte, J. C., Dougherty, K. M., Morris, G. A.,
661 Baumgardner, D., Ladino, L., and Rappenglück, B.: Tropospheric ozone sources and
662 wave activity over Mexico City and Houston during MILAGRO/Intercontinental
663 Transport Experiment (INTEX-B) Ozonesonde Network Study, 2006 (IONS-06). *Atmos.*
664 *Chem. Phys.*, 8, 5113-5125, 2008.

665 Wilks, D., 2011: *Statistical Methods in the Atmospheric Sciences*. Academic Press, 3rd ed., 704
666 pp.

667 Whiteman, C.D., Zhong, S., Bian, X., Fast, J.D., Doran, J.C.: Boundary layer evolution and
668 regional-scale diurnal circulations over the Mexico Basin and Mexican Plateau. *J.*
669 *Geophys Res* 105, 10081-10102, 2000.

670 WHO: Health risks of ozone from long-range transboundary air pollution. World Health
671 Organization, 2008. [available on-line at [http://www.euro.who.int/__data/assets/pdf_file/](http://www.euro.who.int/__data/assets/pdf_file/0005/78647/E91843.pdf)
672 [0005/78647/E91843.pdf](http://www.euro.who.int/__data/assets/pdf_file/0005/78647/E91843.pdf)].

673 Wu, M.-L. C., Schubert, S. D., Suarez, M. J., Pegion, P. J., and Waliser, D. E.: Seasonality and
674 meridional propagation of the MJO. *J. Climate*, 19, 1901-1921, 2006.

675 Zhang, C. Madden-Julian Oscillation. *Rev. Geophys.*, 43, 1-36, 2005.

676 Zhang, C., and Dong, M.: Seasonality in the Madden-Julian Oscillation. *J. Climate*, 17, 3169-
677 3180, 2004.

678 Zhang, Y., Dubey, M. K., Olsen, S. C., Zheng, J., and Zhang, R.: Comparisons of WRF/Chem
679 simulations in Mexico City with ground-based RAMA measurements during the 2006-
680 MILAGRO campaign. *Atmos. Chem. Phys.*, 9, 3777-3798, 2009.

681 **Table captions**

682 Table 1: Station names, locations, period of record, and number of observations.

683

684 Table 2: Relative frequency of extreme ozone days in winter (top two rows) and summer (bottom

685 two rows). A high ozone day was defined as one with a mean afternoon (1200 to 1600 local)

686 ozone anomaly across the 5 observing stations greater than the long-term (1986-2014) 90th

687 percentile. Similarly, a low ozone day was defined as one with a mean afternoon anomaly across

688 the 5 observing stations less than the long-term 10th percentile. Bold values (winter phase 2;

689 summer phase 6) indicate phases with highest mean ozone concentrations in those seasons;

690 italics in italics (winter phase 8; summer phase 1) indicate phases with lowest mean ozone

691 concentrations in those seasons. Number of days (n) in each active phase is given for each

692 season, used to estimate the relative frequency.

693

694 **Figure captions**

695 Figure 1: Locations of RAMA surface ozone stations used in this study (colored dots;

696 abbreviations defined in Table 1) and topographic height (shaded, in m) of the Mexico City

697 metropolitan region. State boundaries shown as black contours. Surface meteorology station at

698 Tacubaya (TCBY) also indicated. The inset in the upper right corner shows the location of

699 Mexico City within Mexico.

700

701 Figure 2: (a) Diurnal cycle of surface ozone concentrations (ppb) at five observing stations

702 (colored lines), as well as the mean (black dotted line) for all seasons, 1986-2014. (b) Diurnal

graciela binimelis d..., 14/10/16 8:16 A.M.

Eliminado: An extreme ozone day was defined as one with mean afternoon hourly (1200 to 1600 local) ozone concentrations at average of all 5 stations either greater than the 90th percentile value or less than the 10th percentile value.

graciela binimelis d..., 14/10/16 8:16 A.M.

Eliminado: values in

709 cycle of surface ozone concentrations for Pedregal (PED; blue lines) and Xalostoc (XAL; red
710 lines) by season from the RAMA network, 1986-2014.

711 Figure 3: Annual cycles of surface ozone concentrations (ppb) for five observing stations for
712 hours 1200-1600 (local time) from the RAMA network, 1986-2014. Observations are smoothed
713 using a 30-day running mean.

714
715 Figure 4: (a) Hourly observations of surface ozone concentrations (ppb) at Pedregal station (PED
716 in Fig. 1). (b) Relative frequencies (in %) of hourly ozone concentrations (ppb) at five observing
717 stations, 1986-2014. (c) Standard anomalies of hourly surface ozone concentrations at PED. (d)
718 Relative frequencies (in %) of standard anomalies of hourly ozone concentrations at five
719 observing stations from the RAMA network, 1986-2014.

720
721 Figure 5: (a) Height (contoured, in m), height anomalies (shaded, in m), and mean winds
722 (vectors) at 250-hPa for winter (DJF) days with standard anomalies of afternoon (1200 to 1600
723 local time) surface ozone at the five observing stations (Fig. 1) below the 10th percentile. (b)-(d)
724 Anomalies (in %) of total cloud fraction, high cloud fraction, and low cloud fraction,
725 respectively, for the same winter days with standard anomalies of afternoon surface ozone
726 concentrations below the 10th percentile. (e)-(h) Same as in (a)-(d), but for winter days with
727 mean afternoon surface ozone concentrations above the 90th percentile. Percentile calculations
728 based on hourly observations from 1986-2014. Height, wind, and cloud fraction data from ERA-
729 Interim; ozone concentrations from RAMA stations.

730
731 Figure 6: As in Figure 5, but for summer (JJA) days.

732

733 Figure 7: Mean standard anomalies of midday (hours 12-16 local time) surface ozone
734 concentrations by active MJO phase for (a) annual, (b) DJF, and (c) JJA. Stations indicated by
735 line color. Error bars indicate largest and smallest standard anomaly values for all stations;
736 dashed black curve indicates mean value. All surface ozone observations from the RAMA
737 network, 1986-2014. (d) Standard anomalies of UV radiation (blue curves) and total cloud
738 fraction (black curves) for each active MJO phase for the entire year. (e) and (f) Same as panel
739 (d) but for DJF and JJA, respectively. UV and cloud fraction data from ERA-Interim reanalysis,
740 1986-2014, for the grid closest to Mexico City.

741

742 Figure 8: Composites of 250-hPa height (in m), height anomaly (in m), and mean wind (a), and
743 total cloud fraction (in %; b), high cloud fraction (in %; c), and low cloud fraction (in %; d) for
744 winter days in active MJO phase 8. (e)-(h) Same as (a)-(d) but for winter days in active MJO
745 phase 2. Phases 8 and 2 were the phases with lowest and highest respective winter ozone
746 concentrations in Mexico City.

747

748 Figure 9: As in Figure 8, but for summer days in active MJO phase 1 (a-d) and active MJO phase
749 6 (e-h). Phases 1 and 6 were the phases with lowest and highest respective summer ozone
750 concentrations in Mexico City.

751

752 Figure 10: Mean 10-m winds at Tacubaya station (TCBY in Fig. 1) at 1800 UTC (1200 local
753 time). Mean surface wind vectors for each season, DJF and JJA, are on row one and indicated by
754 red arrows. Mean (black arrows) and anomaly (blue arrows) vectors for the MJO phases

graciela binimelis d..., 12/10/16 2:01 P.M.
Eliminado: F

756 associated with lowest surface ozone (phase 8 in DJF and phase 1 in JJA) are on the middle row.
757 Mean (black arrows) and anomaly (blue arrows) vectors for the MJO phases associated with
758 highest surface ozone (phase 2 in DJF and phase 6 in JJA) are on the bottom row. Note that the
759 mean winds for low ozone in DJF and high ozone in JJA are very similar to the seasonal mean
760 winds, so the anomaly (blue) vector is very small. All wind data are from NOAA National
761 Centers from Environmental Information, 1986-2014.

Table 1: Station names, locations, period of record, and number and type of observations.

Station name	Abbreviation	Latitude (°N)	Longitude (°W)	Elevation (m)	Period of record	Variable	Number of observations	Frequency of observation
Xalostoc	XAL	19.3	-99.2	2326	1986 to 2014	Surface O ₃	221472	Hourly
Tlalnepantla	TLA	19.4	-99.1	2245	1986 to 2014	Surface O ₃	230992	Hourly
Merced	MER	19.5	-99.1	2160	1986 to 2014	Surface O ₃	219404	Hourly
Pedregal	PED	19.5	-99.2	2311	1986 to 2014	Surface O ₃	217009	Hourly
UAM-Iztapalapa	UIZ	19.4	-99.1	2221	1986 to 2014	Surface O ₃	194224	Hourly
Tacubaya	TCBY	19.4	-99.2	2313	1986 to 2014	Surface wind	7398	Daily (at 1200 local)

762

763

Table 2. Relative frequency of extreme (high or low) ozone days in winter (top two rows) and summer (bottom two rows). A high ozone day was defined as one with a mean afternoon (1200 to 1600 local) ozone anomaly across the 5 observing stations greater than the long-term (1986-2014) 90th percentile. Similarly, a low ozone day was defined as one with a mean afternoon anomaly across the 5 observing stations less than the long-term 10th percentile. Bold values (winter phase 2; summer phase 6) indicate phases with highest mean O₃ concentrations in those seasons; italics values (winter phase 8; summer phase 1) indicate phases with lowest mean O₃ concentrations in those seasons. Number of days (n) in each active phase is given for each season, used to estimate the relative frequency.

	Phase 1 n=134	Phase 2 n=169	Phase 3 n=249	Phase 4 n=222	Phase 5 n=226	Phase 6 n=254	Phase 7 n=282	Phase 8 n=187
Winter (DJF)								
Relative frequency of days with O ₃ concentration greater than the 90th percentile	9.7%	10.1%	7.6%	8.1%	12.8%	9.8%	12.4%	8.6%
Relative frequency of days with O ₃ concentration less than the 10th percentile	9.0%	7.1%	7.2%	8.1%	7.5%	9.8%	12.4%	<i>13.9%</i>
Summer (JJA)								
Relative frequency of days with O ₃ concentration greater than the 90th percentile	8.6%	6.7%	3.6%	10.5%	9.7%	11.7%	11.6%	8.7%
Relative frequency of days with O ₃ concentration less than the 10th percentile	<i>17.1%</i>	9.0%	10.7%	4.4%	5.5%	3.7%	9.1%	14.9%

Table 2: Relative frequency of e ozone day was defined as one w stations either greater than the 90 summer phase 6) indicate phases: summer phase 1) indicate phases: active phase is given for each se

Winter (DJF)

Relative frequency of days with concentration greater than the 90

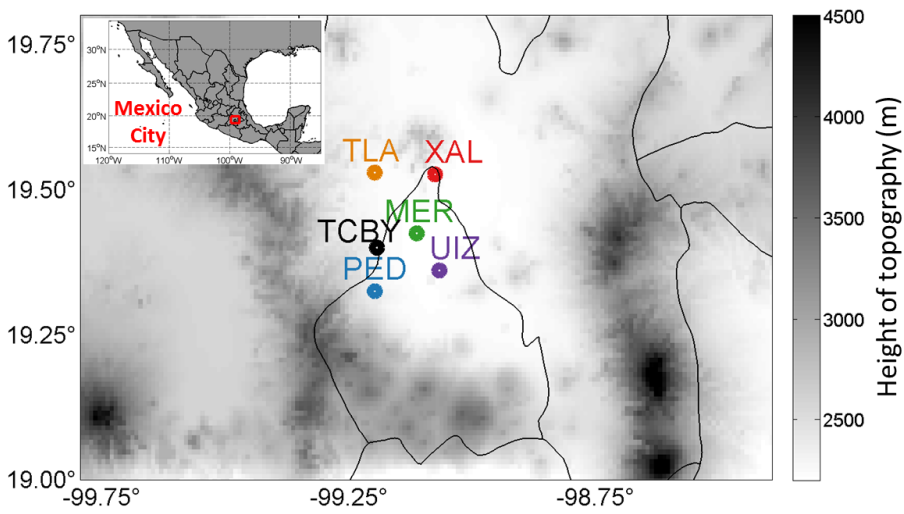
Relative frequency of days with C concentration less than the 10th J

Summer (JJA)

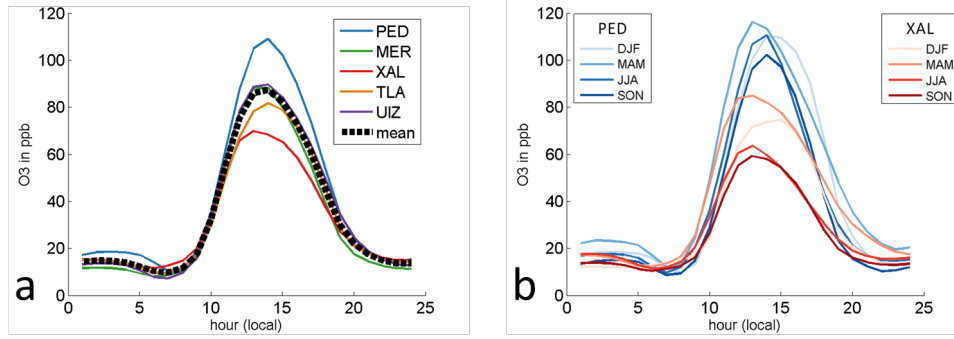
Relative frequency of days with concentration greater than the 90

Relative frequency of days with concentration less than the 10th J

Eliminado:

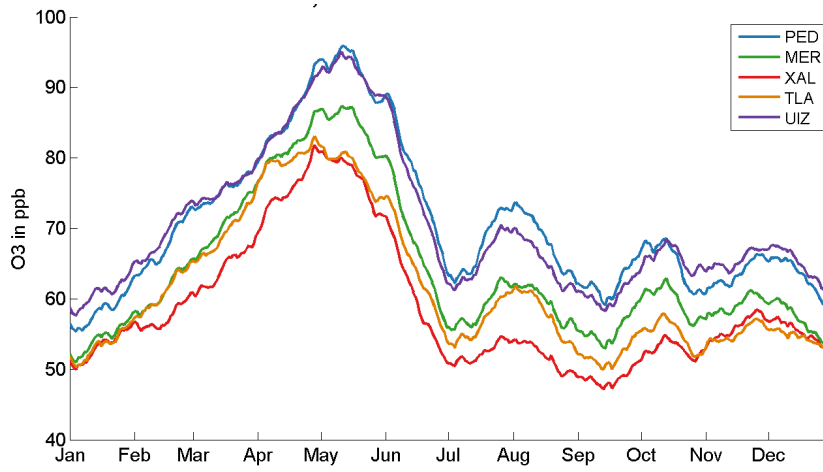


767
 768 **Figure 1:** Locations of RAMA surface ozone stations used in this study (colored dots;
 769 abbreviations defined in Table 1) and topographic height (shaded, in m) of the Mexico City
 770 metropolitan region. State boundaries shown as black contours. Surface meteorology station at
 771 Tacubaya (TCBY) also indicated. The inset in the upper right corner shows the location of
 772 Mexico City within Mexico.

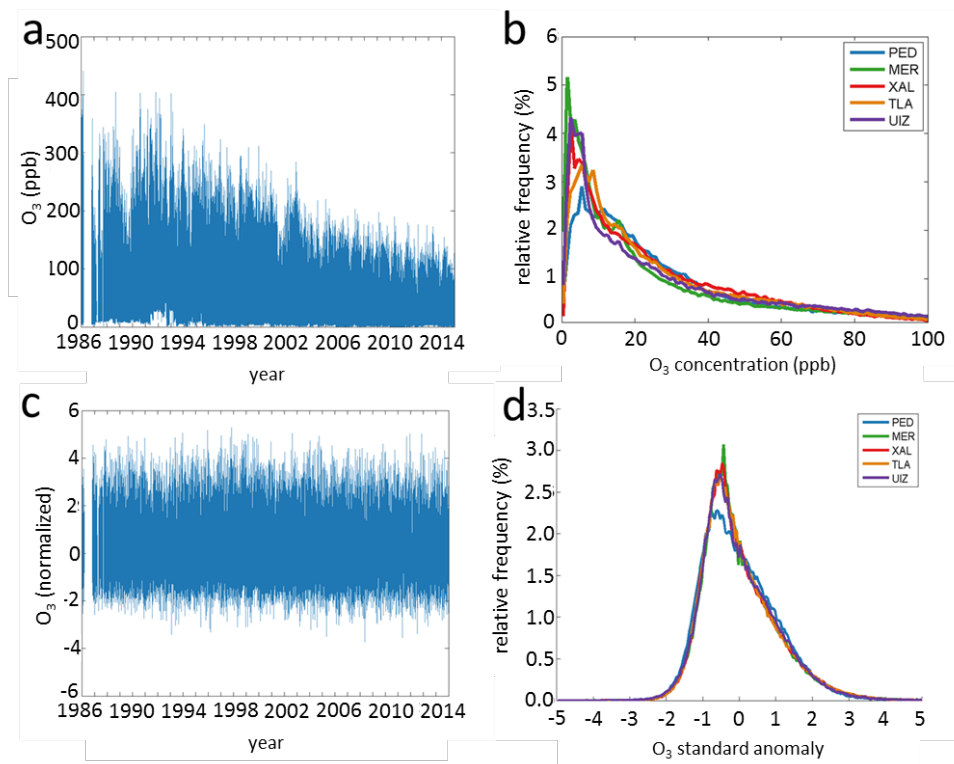


773

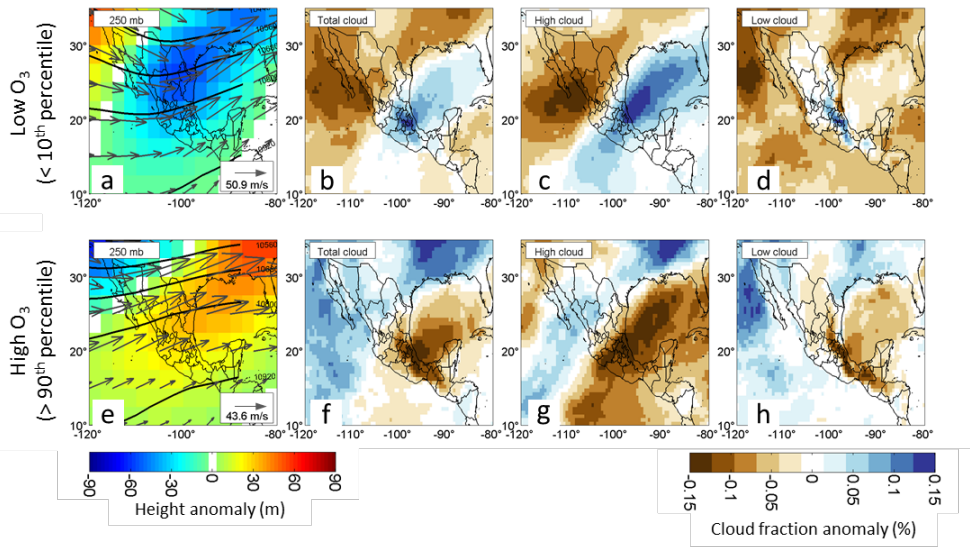
774 **Figure 2:** (a) Diurnal cycle of surface ozone concentrations (ppb) at five observing stations
 775 (colored lines), as well as the mean (black dotted line) for all seasons, 1986-2014. (b) Diurnal
 776 cycle of surface ozone concentrations for Pedregal (PED; blue lines) and Xalostoc (XAL; red
 777 lines) by season from the RAMA network, 1986-2014.



778
779 **Figure 3:** Annual cycles of surface ozone concentrations (ppb) for five observing stations for
780 hours 1200-1600 (local time) from the RAMA network, 1986-2014. Observations are smoothed
781 using a 30-day running mean.

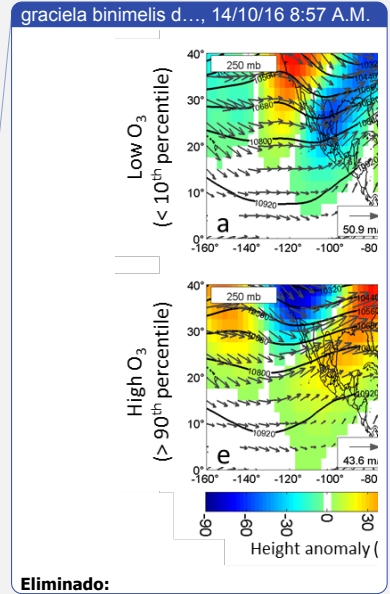


782
 783 **Figure 4:** (a) Hourly observations of surface ozone concentrations (ppb) at Pedregal station
 784 (PED in Fig. 1). (b) Relative frequencies (in %) of hourly ozone concentrations (ppb) at five
 785 observing stations, 1986-2014. (c) Standard anomalies of hourly surface ozone concentrations at
 786 PED. (d) Relative frequencies (in %) of standard anomalies of hourly ozone concentrations at
 787 five observing stations from the RAMA network, 1986-2014.

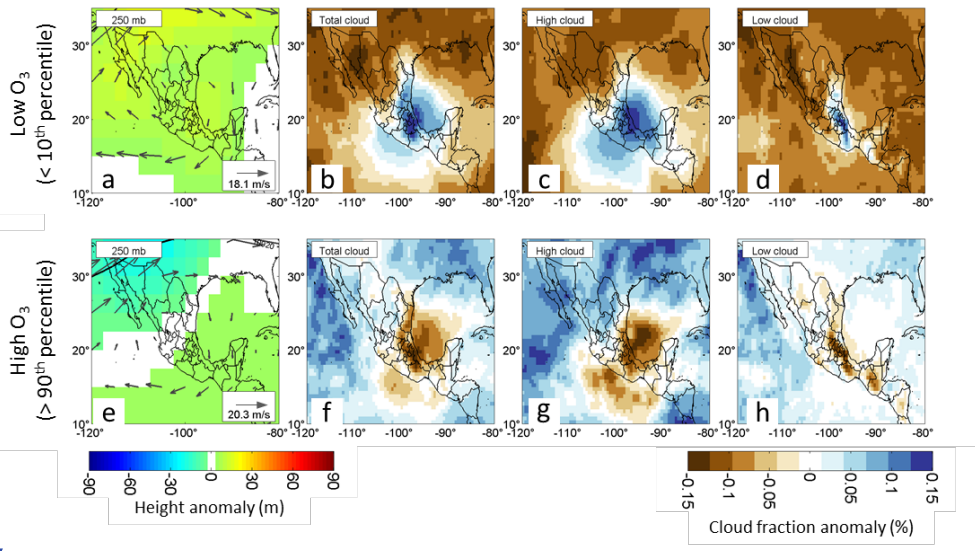


788

789 **Figure 5:** (a) Height (contoured, in m), height anomalies (shaded, in m), and mean winds
 790 (vectors) at 250-hPa for winter (DJF) days with standard anomalies of afternoon (1200 to 1600
 791 local time) surface ozone at the five observing stations (Fig. 1) below the 10th percentile. (b)-(d)
 792 Anomalies (in %) of total cloud fraction, high cloud fraction, and low cloud fraction,
 793 respectively, for the same winter days with standard anomalies of afternoon surface ozone
 794 concentrations below the 10th percentile. (e)-(h) Same as in (a)-(d), but for winter days with
 795 mean afternoon surface ozone concentrations above the 90th percentile. Percentile calculations
 796 based on hourly observations from 1986-2014. Maximum wind speed (in m s^{-1}) is given in
 797 lower-right corner of (a) and (e). Height, wind, and cloud fraction data are from ERA-Interim
 798 reanalysis.

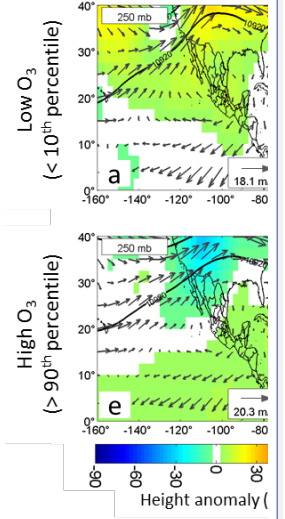


Eliminado:

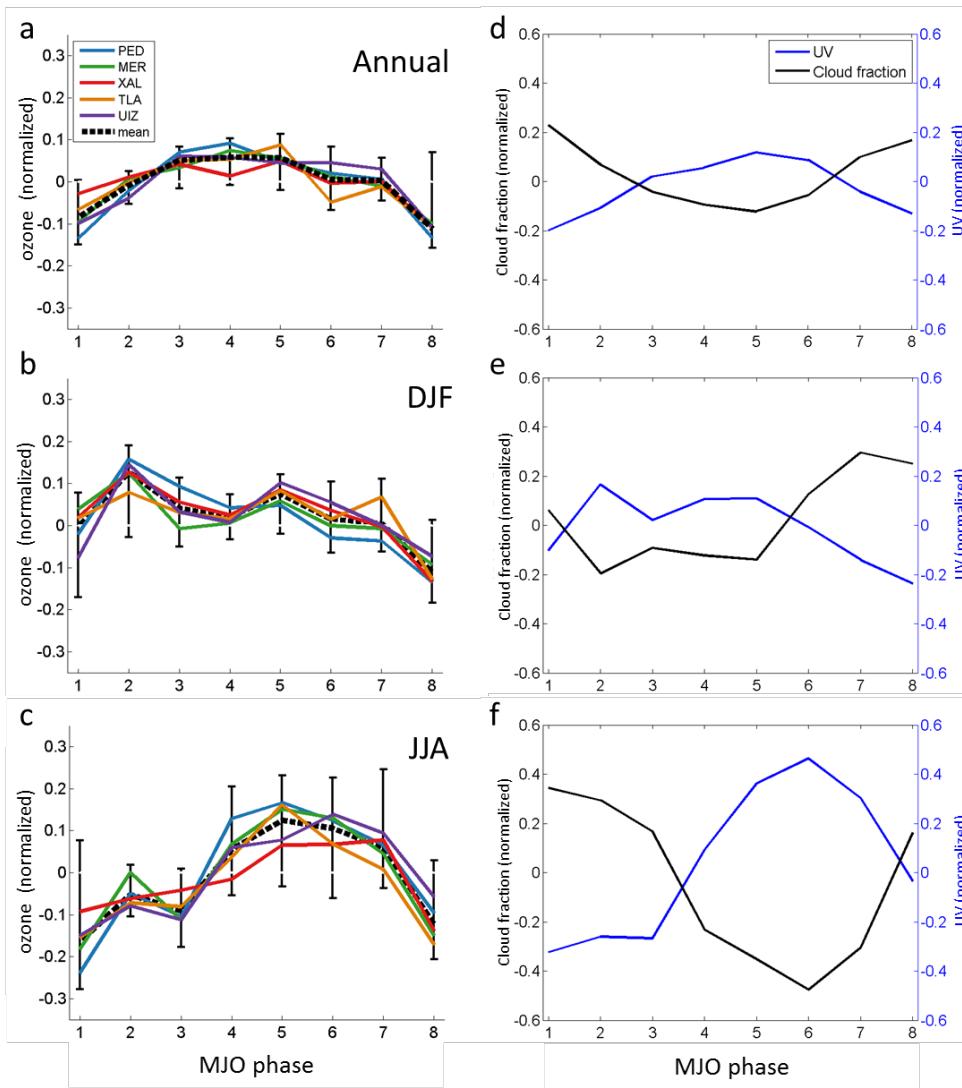


800

801 **Figure 6:** As in Figure 5, but for summer (JJA) days.



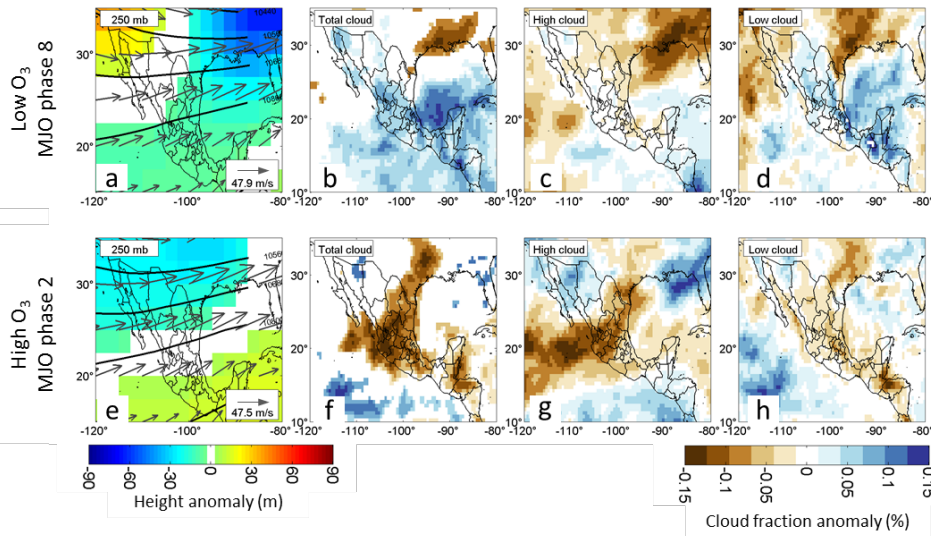
Eliminado:



803
 804 **Figure 7:** Mean standard anomalies of midday (hours 12-16 local time) surface ozone
 805 concentrations by active MJO phase for (a) annual, (b) DJF, and (c) JJA. Stations indicated by
 806 line color. Error bars indicate largest and smallest standard anomaly values for all stations;
 807 dashed black curves in (a)-(c) indicate mean values of all 5 observing stations. All surface ozone

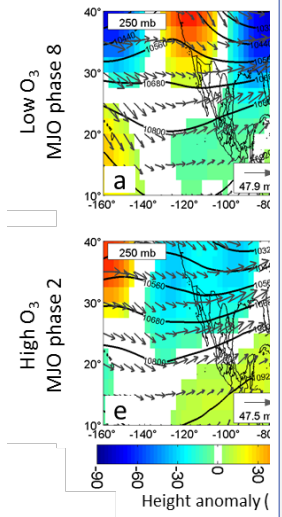
808 observations from the RAMA network, 1986-2014. (d) Standard anomalies of UV radiation (blue
809 curves) and total cloud fraction (black curves) for each active MJO phase for the entire year. (e)
810 and (f): same as panel (d) but for DJF and JJA, respectively. UV and cloud fraction data from
811 ERA-Interim reanalysis, 1986-2014, for the grid closest to Mexico City.

812

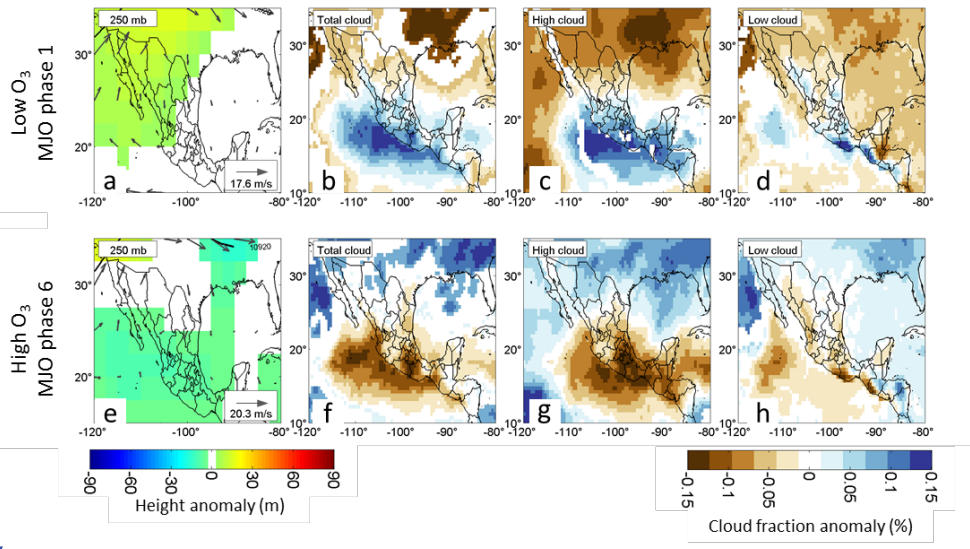


813

814 **Figure 8:** Composites of 250-hPa height (in m), height anomaly (in m), and mean wind (a), and
 815 total cloud fraction (in %; b), high cloud fraction (in %; c), and low cloud fraction (in %; d) for
 816 winter days in active MJO phase 8. (e)-(h) Same as (a)-(d) but for winter days in active MJO
 817 phase 2. Maximum wind speed (in m s^{-1}) is given in lower-right corner of (a) and (e). Phases 8
 818 and 2 were the phases with lowest and highest respective winter ozone concentrations in Mexico
 819 City. Height, wind, and cloud fraction data are from ERA-Interim reanalysis.

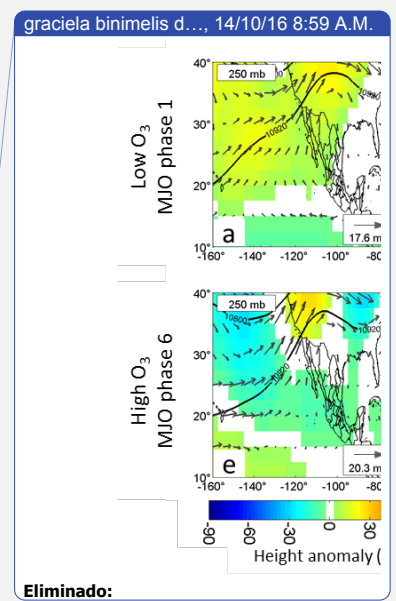


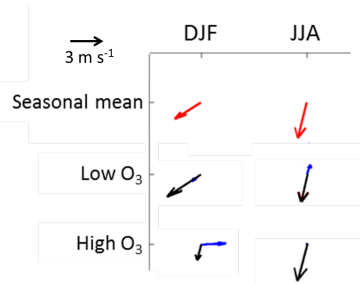
Eliminado:



821

822 **Figure 9:** As in Figure 8, but for summer days in active MJO phase 1 (a-d) and active MJO
 823 phase 6 (e-h). Phases 1 and 6 were the phases with lowest and highest respective summer ozone
 824 concentrations in Mexico City.





826

827 **Figure 10:** Mean 10-m winds at Tacubaya station (TCBY in Fig. 1) at 1800 UTC (1200 local

828 time). Mean surface wind vectors for each season, DJF and JJA, are on row one and indicated by

829 red arrows. Mean (black arrows) and anomaly (blue arrows) vectors for the MJO phases

830 associated with lowest surface ozone (phase 8 in DJF and phase 1 in JJA) are on the middle row.

831 Mean (black arrows) and anomaly (blue arrows) vectors for the MJO phases associated with

832 highest surface ozone (phase 2 in DJF and phase 6 in JJA) are on the bottom row. Note that the

833 mean winds for low ozone in DJF and high ozone in JJA are very similar to the seasonal mean

834 winds, so the anomaly (blue) vector is very small. All wind data are from NOAA National

835 Centers from Environmental Information, 1986-2014.

graciela binimelis d..., 12/10/16 2:01 P.M.
Eliminado: F